Design of a Low Shear Hydrofoil through the use of Computational Fluid Dynamics and Multi-Objective Design Optimization.

Spogis, N.[1], Nunhez, J. R[2].

[1] ESSS, ITC – INTERNATIONAL TRADE CENTER - Rua do Rocio, 423 10 andar conj.1001/1002,

Vila Olímpia – CEP: 04552-000 – São Paulo– SP – Brazil – Phone: + (55) (11) 3017-5191

[2] Faculdade de Engenharia Química, Departamento de Processos Químicos, Unicamp

Universidade Estadual de Campinas, Cidade Universitária Zeferino Vaz,

CEP: 13083-970 – Campinas – SP – Brazil – Phone: + (55) (19) 3521-3967

Abstract

The project of chemical processes and equipments is a task that demands a significant experimental support and a great number of prototypes and tests. Aiming at reducing the development time, ANSYS-CFX tools have been successfully coupled to modeFRONTIER so as to lead to an optimal design of a high efficiency impeller for flow-controlled, low viscosity applications.

The analysis of impeller shape performance was carried out with the SST (Shear-Stress Transport) model coupled with the streamline curvature turbulence model. This model combines the advantages from the $\kappa-\varepsilon$ and $\kappa-\omega$ models, ensuring proper relation between turbulent stress and turbulent kinetic energy and allowing accurate and robust prediction of the impeller blade flow separation. The Multiple Frames of Reference and the Frozen Rotor Frame Change model were used in order to investigate the rotor/stator interaction inside the mixing vessel.

A robust stochastic algorithm was used for the automatic multi-objective constrained shape design process. The multi-objective function has seven design variables, two nonlinear constraints, and two objective functions. Simultaneous increase of the pumping impeller capacity and mixing vessel homogeneity were achieved using this method.

---

1 Author to whom all correspondence should be addressed.

1.   Introduction

Mixing vessels are widely used in the chemical, petrochemical, pharmaceutical, biotechnological, and food processing industries to optimize mixing and/or heat transfer. Mixing must be efficient, precise and reproducible to ensure optimum product quality. Quantities of interest may include mixing times, gas hold-up, power draw, local shear and strain rates, and solids distribution.

In chemical industry, for example, one is very often faced with the problem of mixing reacting substances as fast as possible in order to achieve an efficient reaction. In this case, an impeller which produces a highly turbulent flow is needed to reduce segregation and minimize the mass and energy transport limitation for the chemical reaction.

On the other hand, in biochemistry it is often necessary to suspend microorganisms in bioreactors. This has to be done very carefully without exposing the microorganism to high shear rates that can lead to the destruction of the cells.

Other Macro-level mixing aspect is related to how the flow pattern generated by the impeller affects both the suspension and solid particles incorporation and distribution within the vessel. Parameters that affect Liquid-Solid mixing are the shape of the solids, solid size distribution, solid concentration, solid density, and liquid density and viscosity.

The quality of the solid distribution includes the description of fillets, on bottom motion, off bottom motion, and uniform solid suspension. These effects are very important in some mixing application examples as in the mining industry. Some examples are rubber crumb, crystallization, precipitations and others. Abrasion and impeller wear are important factors to consider in solid-liquid mixing.

Besides the mixing properties, there are also some important economic issues involved. The minimization of the amount of power consumption to ensure certain mixing conditions is one of the issues. The cost of the impeller and vessel materials, the lifetime of the equipment and the breakdown security system are also important.

All the above mentioned aspects depend strongly on various geometric impeller and vessel parameters as well as on the rotational speed and fluid properties.

The variety of mixing applications has led to a tremendous number of different types of impeller and vessels which are in use nowadays. Due to the great amount of influencing factors on the impeller performance, it is very difficult to select a "good" impeller design for a specific process for the criteria indicated above. Hence, experimental investigations are usually very costly and time consuming. The application of Computational Fluid Dynamics (CFD) to address to all these needs results in a faster and lower cost design, reducing experiments and providing a more reliable scale-up. This also gives a better understanding of the processes, leading to higher yields and reduced waste.

In this study, the numerical investigation of the flow of a stirred vessel using a CFD approach coupled with a Multi-Objective Design Optimization method is presented and results indicate it can be a very useful tool, which can offer new possibilities for a higher product quality, cost reduction and power consumption minimization.

The ANSYS CFX software has been chosen for the numerical CFD results. ANSYS ICEM CFD has been chosen for the Geometry and Mesh generation process in order to provide sophisticated geometry acquisition, mesh generation, mesh editing and a wide variety of solver outputs. The built-in geometry creation of the mesh generating software, its highly automated batch processing and the scripting framework has been successfully incorporated inside modeFRONTIER. ModeFRONTIER models range from gradient-based methods to genetic algorithms. It easily specifies objective functions and defines variables. For this work factors that influence the impeller geometry shape will be investigated. This optimization software in effect

becomes a link between the CAE tools (ICEM and CFX), performing the optimization procedure by modifying the value assigned to the input variables, and monitoring the outputs.

2.   Basic numerical concepts

In the following sections, a brief introduction of the CFD model is considered and a description of the employed numerical tools is also given. Then the coupling of the models within the commercial program (modeFRONTIER) is discussed.

2.1.   Governing equations for fluid flow

The set of equations solved by ANSYS CFX are the unsteady Navier-Stokes equations in their conservation form and the mass conservation equation. The instantaneous equations of mass, momentum and energy conservation can be written as follows in a stationary frame:

The Continuity Equation

$$\frac{\partial \rho}{\partial t} + \nabla \bullet (\rho U) = 0 \qquad \text{Eq. 1}$$

The Momentum Equations

$$\frac{\partial (\rho U)}{\partial t} + \nabla \bullet (\rho U \otimes U) = -\nabla p + \nabla \bullet \tau + S_m \qquad \text{Eq. 2}$$

Where the stress tensor, τ, is related to the strain rate by

$$\tau = \mu \left(\nabla U + (\nabla U)^T - \frac{2}{3} \delta \nabla \bullet U \right) \qquad \text{Eq. 3}$$

For flows in a rotating frame of reference, rotating at a constant angular velocity, additional sources of momentum are required to account for the effects of the Coriolis force and the centrifugal force:

$$S_{M,rot} = S_{Cor} + S_{cfg} \qquad \text{Eq. 4}$$

$$S_{Cor} = -2\rho\omega \times U \qquad \text{Eq. 5}$$

$$S_{cfg} = -\rho\omega \times (\omega \times r) \qquad \text{Eq. 6}$$

Where r is the location vector and is the relative frame velocity (i.e., the rotating frame velocity for a rotating frame of reference).

2.1.1. Alternate rotation model

The Alternate Rotation Model is a model developed for the advection term in the momentum equations. Instead of solving for the relative velocity, the flow solver solves for the absolute frame velocity.

2.1.2. Frozen rotor model

The Frozen Rotor model treats the flow from one component to the next by changing the frame of reference while maintaining the relative position of the components. In this study an 1/3 periodicity has been used to reduce the number of components to a subset that has approximately the same pitch ratio of the full geometry.

2.2. Turbulence modeling

The ANSYS CFX Shear Stress Transport (SST) model was chosen since it combines advantages from the k-e and k-w models, ensuring proper relation between turbulent stress and turbulent kinetic energy (SST) and it also allows accurate and robust prediction of problems with flow separation. This aspect is important in this project since it is important that there is no boundary layer separation in the modeled impeller.

2.2.1. Mesh resolution near the wall

In these simulations there is no interested in solving for the boundary layer profile so the ANSYS CFX model is set up to use wall functions for the near wall region. Although wall functions are extremely useful in reducing computational load, there is a limitation of its application to situations in which the model is valid and care should be taken to ensure that their use is appropriate.

Accurate near wall treatment is of high importance for accurate boundary layer (wall bounded flow) and heat transfer simulations. The treatment in CFX combines the advantages of low-Reynolds number models and wall functions. It is therefore independent of the near wall resolution, which is not the case for standard formulations.

2.2.2. Vessel parameterization

A schematic draw of the vessel configuration is shown in Figure 1. The system consists of a torispherical-bottomed cylindrical vessel with diameter T and height H, which equals the height of the liquid. The off-bottom clearance if constant and equal H/4.

The torispherical 100-6 head has a crown radius of 100% (or equal to) the diameter of the head with a knuckle radius of 6% of the diameter of the head. The shaft of the impeller is concentric with the axis of the vessel. The actual geometrical parameters, which are considered as a standard configuration, are summarized in Table 1. The working Newtonian fluid is water at 25^0 C, with density ρ = 997.0 kg/m³ and viscosity μ= 0.8899 cP.

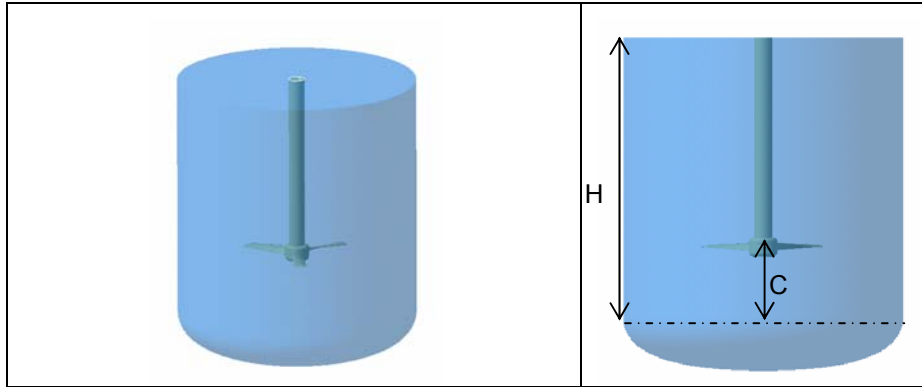| Parameters	Parameter Value
Tank diameter	T = 1m
Height of the liquid	$H= T$ = 1m
Bottom clearance	$C=H/4$ = 0.25m
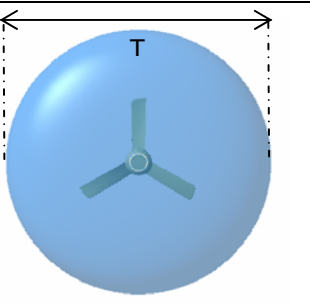
Figure 1 – Vessel schematic draw

2.2.3. Impeller parameterization

The optimization of impeller blades requires a representation of an impeller blade that should be flexible enough to represent a very wide range of potential impeller shapes. Conversely it should be compact enough to allow an efficient storage and manipulation data for a wide variety of viable breeding *population* of candidate impellers.

Changes on the efficiency of the impeller are produced by a wide number of factors, notably adjustments to the helix angle, the angle between the resultant relative velocity and the blade rotation direction, and also to the blade pitch. Very small pitch and helix angles give a good performance against resistance but provide little thrust and also little pumping, while larger angles have the opposite effect.

The best helix angle is when the impeller blade is acting as a wing producing much more lift than drag, roughly 45 degrees in practice. However due to the shape of the impeller, only part of the blade can actually be operating at peak efficiency. The outer part of the impeller blade produces the most pumping and so the blade is positioned at a pitch that gives optimum angle to that portion. Since a large portion of the blade is therefore at an inefficient angle, the inboard ends of the impeller blade are hidden by a streamlined spinner to reduce the resistance torque that would otherwise be created. Very high efficiency pumping impellers are similar in its airfoil section to a low drag wing and, as such, need an optimum angle of attack to work properly. An impeller working at a pitch angle of 45 degrees, at high rotational speeds presents a very high angle of attack will be high. There is a need to adjust the impeller pitch angle to alter resistance torque and improve efficiency. A further consideration is the number and the shape of the blades used. Increasing the aspect ratio of the blades reduces drag. However, the amount of pumping produced depends on blade area, so using high aspect blades can lead to the need of an impeller diameter which is unusable.

A further balance is that using a smaller number of blades reduces the interference effects between the blades, but there is a need of sufficient blade area to transmit the available power, so a compromise between these opposing effects is needed. Increasing the number of blades also decreases the amount of work each blade is required to perform.

2.2.4. Impeller blade parameterization

A schematic draw of the impeller configuration is shown in Figure 2. The impeller consists of a twisted blade designed by seven construction parameters: Impeller diameter ratio (D/T), Root chord (R_HD*(D/T)), Tip chord (T_HD*(D/T)), Root chord angle (RCA), Tip chord angle (TCA), Root profile (RP) and Tip profile (TP).

The newest Low Shear Hydrofoil design has a variable to consider different tip chord angles (TCA). These angles allow for the optimization of axial pumping impellers on the basis of flow and shear. Previously, only hydrofoils with a single TCA were used.

This new hydrofoil impeller has been designed to maximize solid dispersion in stirred vessels at the lowest possible power consumption.
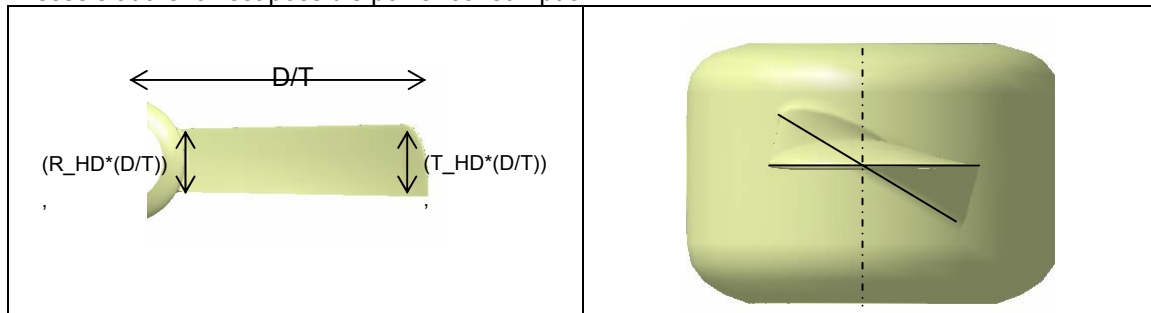

Figure 2 – Impeller schematic draw

2.2.5. Impeller blade airfoils

An airfoil with the shape of a wing or blade is seen at its cross-section. It is passed through a fluid in order to provide either lift or downforce, depending on its application. This force is generated by a pressure gradient. The pressure gradient and the impeller blade size are responsible for the impeller pumping.

Subsonic and Low-Reynolds airfoils have a characteristic shape with a rounded leading edge, followed by a sharp trailing edge, and often with camber. The characteristics of these airfoils and the criteria adopted for their selection are discussed in the following sections.

2.2.5.1. Low-speed airfoils

A most comprehensive source of low-speed airfoil geometries and performance data is provided by Selig et al. (2001) at the University of Illinois at Urbana-Champaign (UIUC). SoarTech Publications distribute compendiums of airfoil coordinates from the UIUC project, the most recent of which is Lyon et al. (1998).

An example of the work performed by UIUC in tackling the problem of designing airfoils for small Wind Turbines is provided by Giguère and Selig (1998), who report on the development of their SG604x set of airfoils. These airfoils feature enhanced lift-to-drag ratios for low Reynolds numbers, and lift and drag curves covering Reynolds numbers from 100,000 to 500,000, derived from experimental wind tunnel tests, along with x-y coordinates for all four airfoils.

2.2.5.2. Rotary wing

Most of the published experimental works for rotary wings are for helicopter rotors, with the "hovering" maneuver being somewhat similar to the mode of operation of impellers in stirred vessels, particularly because the wake shed from the rotor is reminiscent of the coaxial helical vortices shed by the impeller blades and subsequently flowing downstream.

Interesting experimental data for helicopter rotors in hovers is provided by Caradonna and Tung (1981) and Branum and Tung (1997). The latter is particularly a comprehensive study and offers rotor geometry descriptions and detailed surface pressure data tables.

These studies are valuable when validating rotary wing prediction codes because of the lack of similar information available for wind turbines and the similarity in flow generated by hovering helicopter rotors.

Possible validation data is also provided by Wolfe and Ochs (1997). They report on that study a comparison for the predictions of commercially available CFD codes with wind tunnel tests of two common airfoil sections. *Cp* vs. chord data are provided for S809 and NACA0012 airfoils at various angles of attack and Reynolds number ranging from 1×10^6 to 5×10^6.

Other examples of techniques to solve numerically the full Navier-Stokes equations are provided by Hsiao and Pauley (1999) for marine propeller flows and Xu and Sankar (2000) for flows of wind turbines. Conlisk (1997) offers a recent review for the aerodynamic of helicopter rotors which also serves as a general introduction to rotary wing aerodynamics.

2.2.5.3. Airfoil selection

The criteria adopted for the airfoil selection in this study are high lift at low angle of attach, high C_{lmax}, gentle stall characteristics, relative low coefficient of moment, sufficiently low drag, easy manufacturability and good operations at low Reynolds number.

Based on these criteria, four possible airfoils were selected and used as root and tip blade airfoil parameters, as shown in Figure 3:
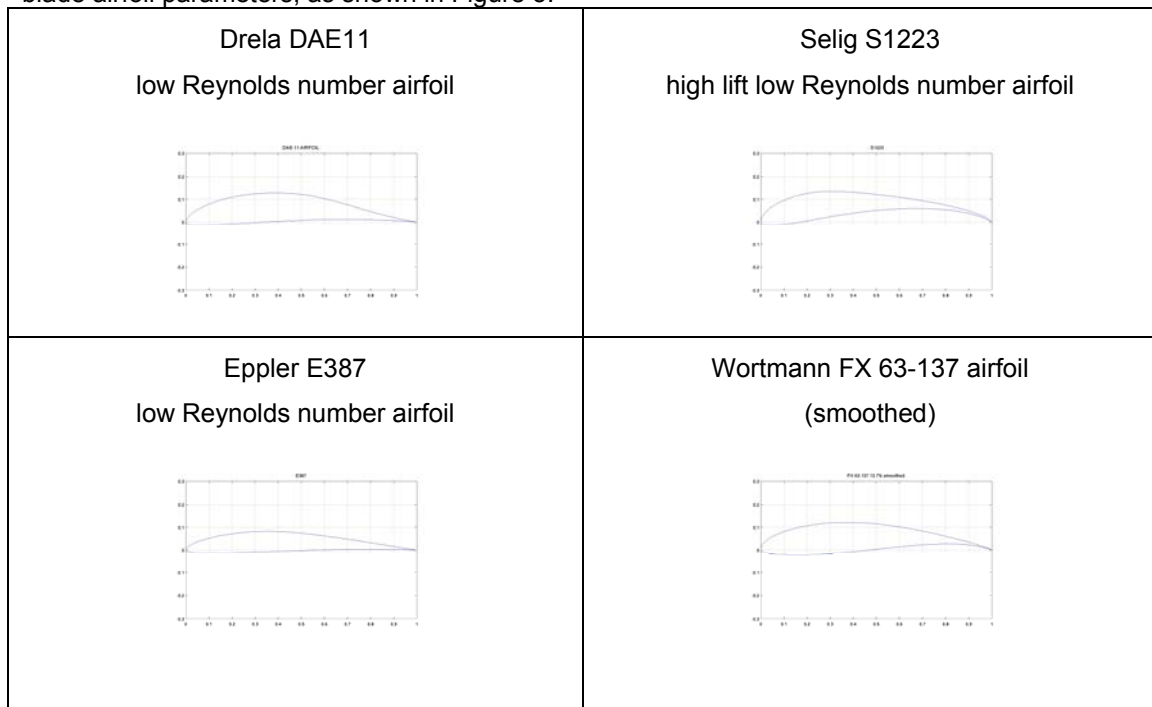
Drela DAE11	Selig S1223
low Reynolds number airfoil	high lift low Reynolds number airfoil
Eppler E387	Wortmann FX 63-137 airfoil
low Reynolds number airfoil	(smoothed)

Figure 3 – Low Reynolds airfoils

2.3. Grid parameterization and generation

One of the most essential issues for the optimal performance of the SST turbulence model with curvature correction is the proper solution of the boundary layer. So two criteria need to be respected in order to generate meshes which satisfy the minimal requirements for accurate boundary layer computations:

- Minimum spacing between nodes in the boundary layer
- Minimum number of nodes in the boundary layer

Below it is shown an estimation of the near wall mesh spacing requirements (Δy), based on simple modifications of the correlations for a flat plate, in terms of Reynolds number, running length, and a y^+ target value.

$$U_\infty = \omega D$$

ω = Angular Velocity
D = Impeller Diameter

Eq. 7

$$\text{Re}_L = \frac{\rho U_\infty L}{\mu}$$

Eq. 8

L = Average Impeller Streamwise

The correlation for the wall shear stress coefficient (cf), is given by:

$$cf = 0.025\,\text{Re}_x^{-1/7}$$

Eq. 9

where x is the distance along the Impeller Streamwise from the leading edge.

The definition of Δy^+ for this estimate is:

$$\Delta y^+ = \frac{\Delta y u_\tau}{\nu}$$

Eq. 10

With Δy being the mesh spacing between the wall and the first node away from it.

Using the definition

$$cf = 2\frac{\rho u_\tau^2}{\rho U_\infty^2} = 2\left(\frac{u_\tau}{U_\infty}\right)^2$$

Eq. 11

u_τ can be eliminated in Eq. 14 to yield:

$$\Delta y = \Delta y^+ \sqrt{\frac{2}{cf}}\frac{\upsilon}{U_\infty}$$

Eq. 12

$$\Delta y = L\Delta y^+ \sqrt{80}\,\text{Re}_x^{1/14}\frac{1}{\text{Re}_L}$$

Eq. 13

Further simplification can be made by assuming that:

$$\text{Re}_x = C\,\text{Re}_L$$

Eq. 14

where C is a constant with a fractional value.

Assuming that $C^{\frac{1}{14}} \approx 1$,, except for very small Re_x, the result is:

$$\Delta y = L\Delta y^+ \sqrt{80}\,\text{Re}_L^{-13/14}$$

Eq. 15

A good mesh should have a minimum number of mesh points inside the boundary layer in order for the turbulence model to work properly. So, an estimation of the boundary layer thickness and the wall normal expansion ratio has been used in order to determine the number of nodes on the boundary layer in the direction normal to the wall.

The boundary layer thickness δ can then be computed from the correlation:

$$\text{Re}_\delta = 0.14\,\text{Re}_x^{6/7}$$

Eq. 16

Eq. 17

$$\delta = 0.14L\,\text{Re}_x^{6/7}\frac{1}{\text{Re}_L}$$

Since the boundary layer for a blunt body does not start with zero thickness at the stagnation point for Re_x, it is safe to assume that Re_δ is some fraction of Re_L. Assuming that it is around 25%:

$$\delta = 0.035 L \mathrm{Re}_L^{-1/7} \qquad \text{Eq. 18}$$

By the use of the sum of n terms of a geometric progression definition for the boundary layer thickness and also for the first layer thickness and the wall normal expansion ratio, the number of nodes in the boundary layer is given by:

$$\delta = 0.035 L \mathrm{Re}_L^{-1/7} = \frac{\Delta y (q^n - 1)}{q - 1} \qquad \text{Eq. 19}$$

Were q is the wall normal expansion ratio and n is the boundary layer nodes. So n can be determined by:

$$n = round \left(\frac{\ln \left(\frac{0.035 L \mathrm{Re}_L^{-1/7}(q-1)}{\Delta y} + 1 \right)}{\ln(q)} \right) \qquad \text{Eq. 20}$$

Respecting these requirements, a tetrahedral mesh was generated by ICEM CFD taking the full advantage of the object oriented unstructured meshing technology. The surface mesh was generated using the Octree approach. The volume mesh was generated by the advanced front and inflation methods and a powerful smoothing algorithm was chosen in order to provide high element quality.

As described above it is very important to solve the boundary layer precisely on the numerical simulations. The accuracy of calculation has been improved by arranging thin prism layers near the wall. ICEM CFD Prism was used in order to generate a good prism boundary layer near the walls. The mesh generated is shown in Figure 4.
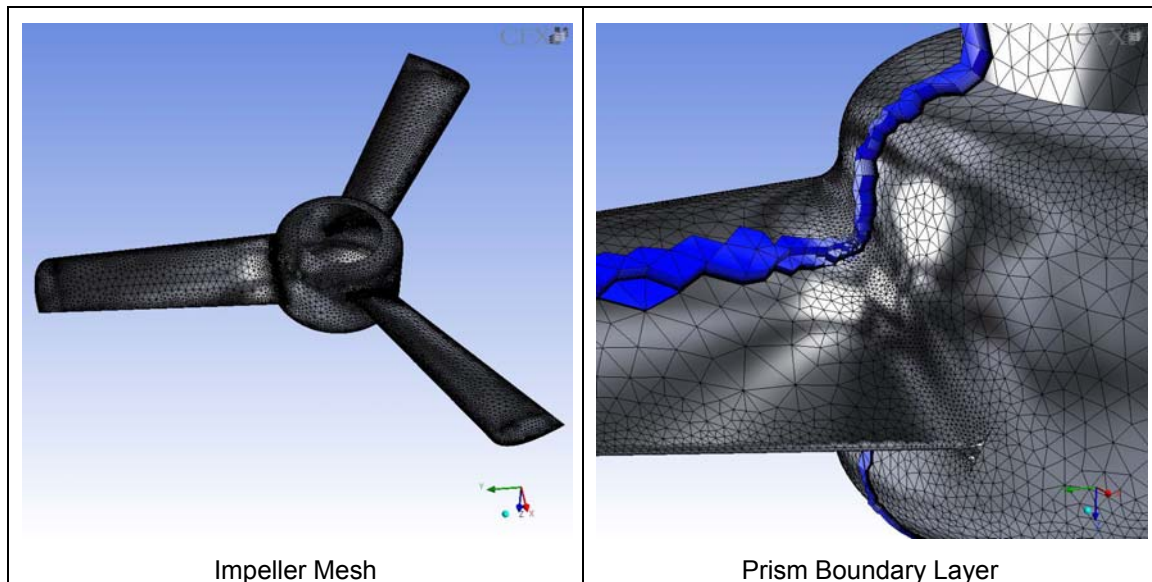

| Impeller Mesh | Prism Boundary Layer |

Figure 4 – Impeller mesh

2.4. Numerical principles of the optimization method

It's well known that classical gradient based algorithms methods use the "direction of improvement" information in order to achieve a fast and accurate convergence towards the optimal solution, but it requires an accurate gradient evaluation.

Holland (1975) is generally credited for the creation of the Genetic Algorithm model and he gives an introduction to the method. He points out that the success of this computational method over other search and optimization techniques, such as simple hill climbing, is due to the ability to properly use *partial solutions* in the optimization problem. ModeFRONTIER has implemented an improved version of Multi-Objective Genetic Algorithm (MOGA-II). It uses a smart multisearch algorithm for robustness and directional crossover for fast convergence. Its efficiency is ruled by its reproduction operators: classical crossover, directional crossover, mutation, and selection.

This project employed this Multi-Objective Genetic Algorithm to determine a Pareto optimal set of impeller blade designs, with each member offering a unique trade-off between the conflicting objectives of energy consumption, increasing of the impeller pumping capacity and increasing in the mixing homogeneity. The Pareto optimal design consists of all the non-dominated solutions possible in the N-dimensional parameter domain being considered, and forms an N-dimensional trade-off surface.

2.5. Control program

The components described in the preceding sections are integrated and coupled to modeFRONTIER which is illustrated schematically in Figure 5.

The optimization procedure involves the following major steps:

1.   **Optimizer:** The optimizer is started and computes a new set of design variables. Afterwards it is turned to a waiting state.

2.   **Geometry and Grid generation:** Getting the signal that the new design variables are available, the grid generation tool (ICEM CFX), becomes active and creates the new geometry and the corresponding numerical grid.

3.   **Flow simulation:** Np calculation: Getting the signal that the new grid is available, the flow solver computes the flow field and estimates de Pumping Number - Nq. This simulation is made using a steady state approach.

4.   **New rotation computation**: With the Nq, impeller diameter and fluid density, a new rotation velocity is calculated in order to conserve the power consumption. This computation is described in the next section (Power Consumption Conservation).

5.   **Steady state flow simulation:** With the new rotation velocity, a new steady state simulation was computed in order to determine a starting value for the next step that will determine the solid distribution.

6.   **Transient solid dispersion:** Estimates the solid distribution in the stirred vessel.

7.   **Post process results:** In this step CFX Post computes the output variables and objective functions for the new geometry, and writes them in an output ASCII file of modeFRONTIER.

8.   **Test of optimizer convergence:** The optimizer decides by a given criteria if the current value of the objective function should be accepted as optimum. If yes, the procedure is finished, if not, the procedure is repeated from step (1).
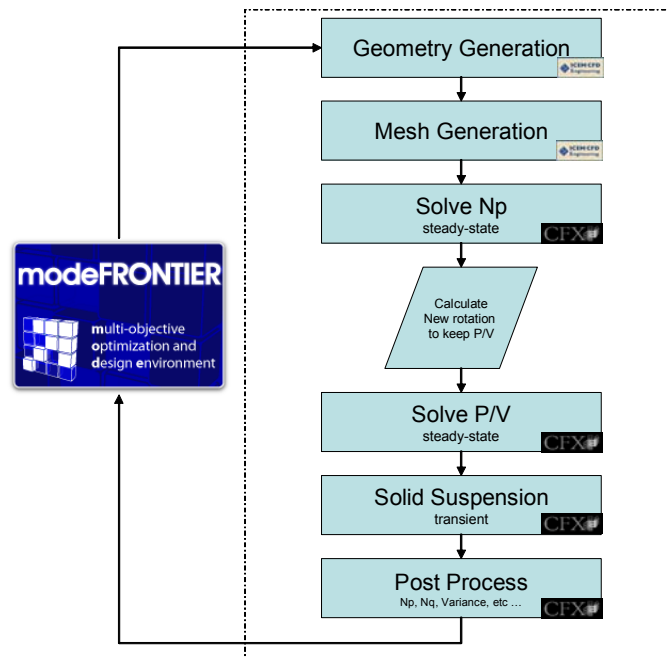
Figure 5 – Schematic illustration of the control program

2.5.1. Power Consumption Conservation

Scale-up based on equal power per volume, P/V, is probably the most commonly used criteria in mixing because it is easily understood and practical. Other advantages of using P/V as scale-up criteria are:1-it correlates as well with mass-transfer characteristics in the mixer; 2- it is conservative enough to provide adequate performance in production scale equipment, particularly when no other strong correlating parameter has been determined from small-scale testing.

As the vessel volume in this optimization is constant, there is only a need to maintain the power consumption constant. As the impeller geometry is not constant, the Power Number (Np), is also not constant, so rotational speed corrections are needed in order to maintain the Power Consumption constant.

A Power Consumption of 2 kW/m³ is required to heavy a solid suspension processes. This value was fixed in the optimization process, so the different impellers generated could be compared only in terms of characteristic flow and its capacity to homogenize the stirred vessel.

The following algorithm was used for steps 3 to 5 of the optimization procedure to maintain the power consumption constant:

1.   Evaluate the Torque

2.   With the blade torque and initial rotation velocity, calculate the Power consumption: $P = \varpi . \mathrm{T}$

3.   With the power consumption, fluid density, initial rotation velocity and impeller diameter, calculate the Power Number: $Np = \dfrac{P}{\rho . N^3 . D^5}$

4.   With the Power Number, impeller diameter, fluid density and the desired Power consumption, a new rotational speed is calculated and used in the step 5 of the optimization procedure:

$$N = \sqrt[3]{\dfrac{P}{\rho . D^5 . Np}}$$

2.5.2. Input variables

Five continuum variables and two discrete variables were used in the impeller blade parameterization, as shown in the Table 2.

Variable	Minimum Value	Maximum Value	Discrete / Continuum
Impeller diameter	0.4	0.5	Continuum
Root chord	0.2	0.2	Continuum
Tip chord	0.1	0.2	Continuum
Root chord angle	20 degrees (related to rotation axis)	70 degrees (related to rotation axis)	Continuum
Tip chord angle	30 degrees (related to rotation axis)	95 degrees (related to rotation axis)	Continuum
Root profile	DAE11, S1223, E387, FX 63-137		Discrete
Tip profile	DAE11, S1223, E387, FX 63-137		Discrete

Table 2 – Input variables

2.5.3. Constraints

Constraint handling is an integral part of any general parameter optimization method. In order to restrict the solution to a restricted area, only two of the defined constraints relate specifically to the creation of "realistic impeller blades" in the optimization problem:

- Tip chord angle <= Root chord angle

- Tip chord <= Root chord

2.5.4. Output variables and objective functions

Ten output variables were used to monitor the mixing efficiency but only two of them were used as an objective function. The pumping effectiveness and the vessel solid concentration variance were used as objective functions. The pumping effectiveness was maximized and the vessel solid concentration variance was minimized.

The vessel solid concentration variance was calculated by the well known statistical formula:

$$s^2 = \frac{1}{n-1} \sum_{i=1}^{n} \left(C_i - \overline{C} \right)^2$$

Eq. 21

Were n is the number of nodes in the mixing vessel mesh.

3. Numerical results

In the following sections it is given a description of the grid requirements and then a discussion of the preliminary investigations of the design space is also given. These sections propose a strategy to reduce computational errors and minimize the computational time required to optimize and design the Low Shear Hydrofoil prototype.

3.1. Grid requirements

Studies of increasing and decreasing the maximum y^+ value in the impeller for values between 0.001 and 1 show that there is almost no effect of these changes on the final solution. Once the maximum y^+ increases to values above 10, the transition onset location begins to move upstream. At a maximum y^+ of 25, the boundary layer is almost completely turbulent. Preliminary investigations also indicate that for y^+ values below 0.001, the transition location appears to move downstream. This is presumably caused by the large surface values of the specific turbulence frequency, which scales with the first grid point height.

The effect of wall normal expansion ratio from a y^+ value of 1 was studied in order to determine the number of cells in the boundary layer. For expansion factors between 1.05 and 1.1, there is no effect on the solution. For larger expansion factors between 1.2 and 1.4, there is a small, but noticeable upstream shift in the transition location.

The effect of the streamwise grid refinement shows that the model was not very sensitive to the number of streamwise nodes. The grid independent solution appears to occur when there are approximately 80 streamwise grid points.

3.2. Preliminary investigations

Preliminary investigations are important in order to determine the behavior and the main characteristics of the problem that is being examined. The aim is to get the most relevant qualitative information from a database of experiments making the smallest possible number of evaluations and building some "knowledge" of the behavior of the objectives and constraints.

The distribution of the initial individuals on the design space is shown in Figure 6.

Initial 2D CFD studies shows that the DAE 11 airfoil provides a better lift/drag relationship and gentle stall characteristics when compared to the other airfoils. In order to minimize the number of input parameters and reduce the computational time requirements, the Root Profile and the Tip Profile was fixed as for DAE 11.
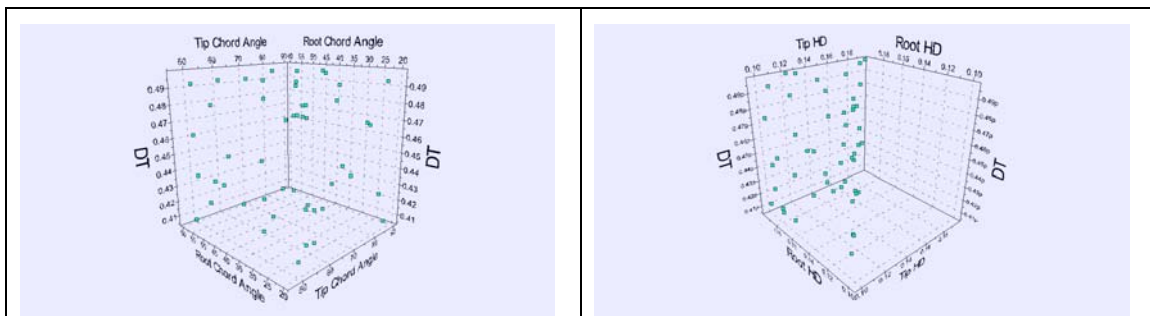

Figure 6 – Design space

Figure 7 shows the relationship between the solid concentration variance and the input parameters (Root Chord Angle, Tip Chord Angle, Impeller Diameter, Root Chord and Tip Chord).
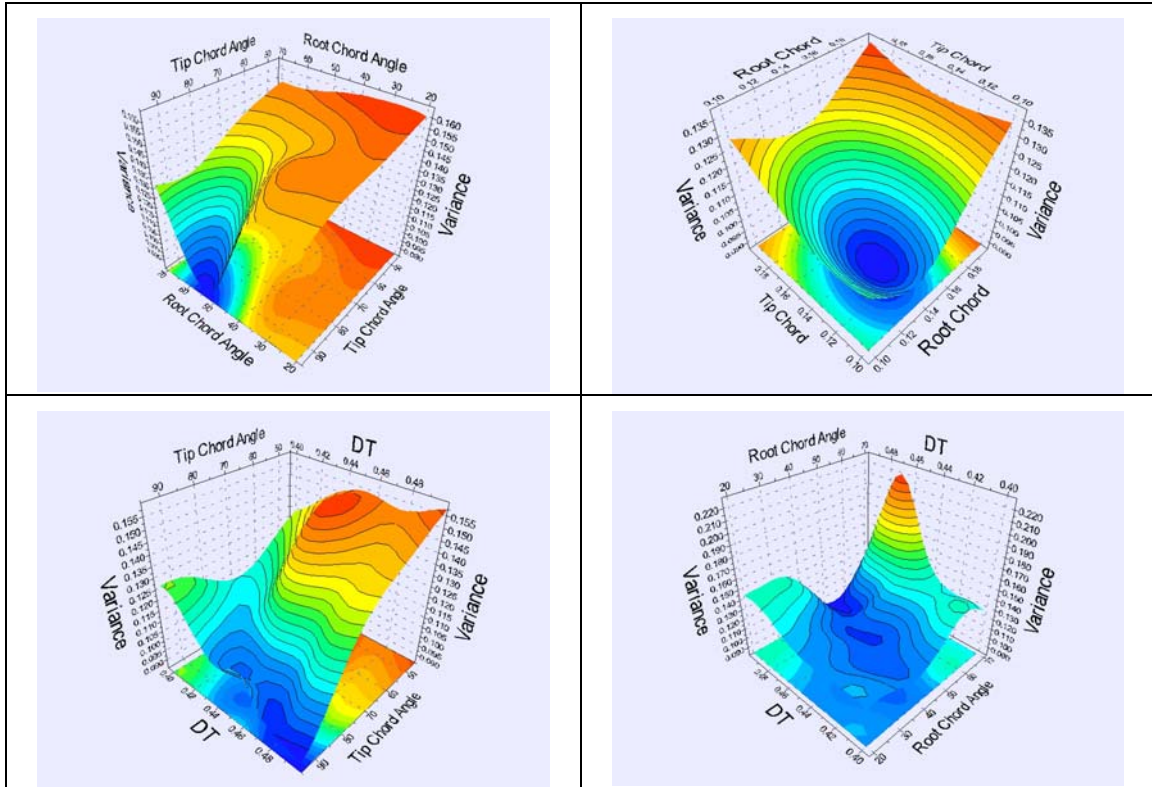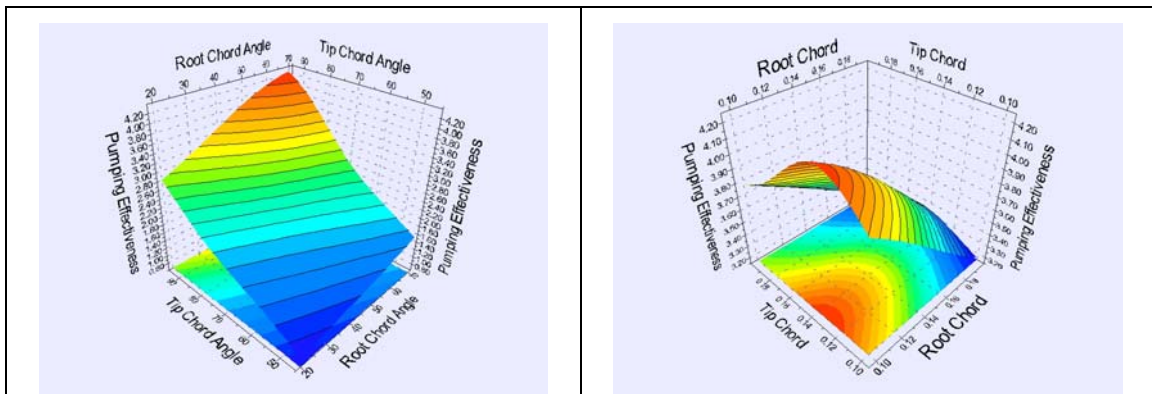
Figure 7 – Response surfaces for vessel solid concentration variance

Figure 8 shows the relationship between the pumping effectiveness and the input parameters (Root Chord Angle, Tip Chord Angle, Impeller Diameter, Root Chord and Tip Chord).
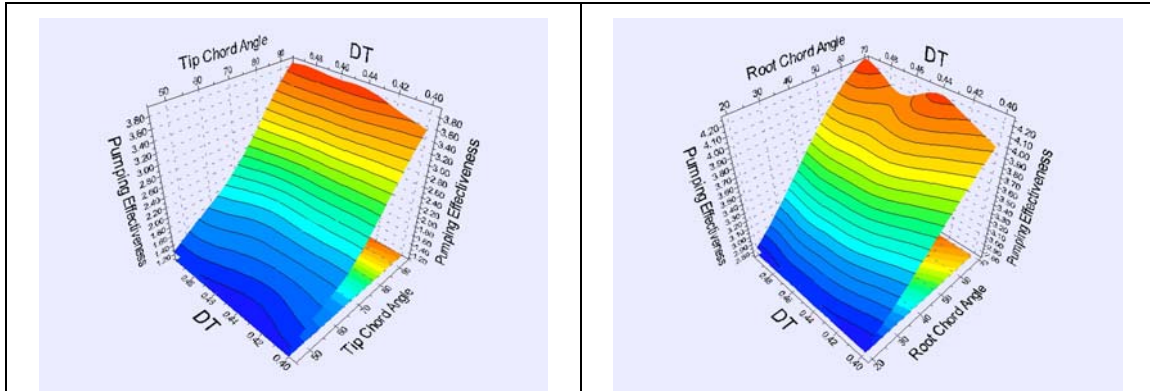
**Figure 8 – Response surfaces for pumping effectiveness**

4. Optimization results

It is important to mention that the computational requirements for one optimization step takes approximately 5.2 hours of computing time on a two processor AMD Athlon™ MP 2800+ machine, 2 GB RAM. The optimization process was configured so as to guarantee the robustness of the calculation. The optimization method arrived at some very interesting results and it required only fifteen generations of thirty individuals (450 optimization cycles), resulting in about 98 days of computing time.

The performed evaluations allowed for a establishment of a general tendency and for the definition of the influence of each of the parameters on the estimated values. Furthermore, the solid concentration variance was reduced by 48.5% and the pumping effectiveness increased by 410.2%, when compared to the performance of a standard pitched blade impeller (45 degrees constant Tip Chord Angle – PTB45).

The initial pitched blade impeller (Constant Tip Chord Angle – 45 degrees), has a low discard angle and a weak solid suspension. The pumping effectiveness is very low due to some radial velocity discharge angle of the PTB45. This flow is generated by a boundary layer separation and there is a blade stall due the high tip chord angle.

The velocity vector plot, the solid concentration distribution, the velocity distribution and the 3D streamlines are shown in Figure 9 .
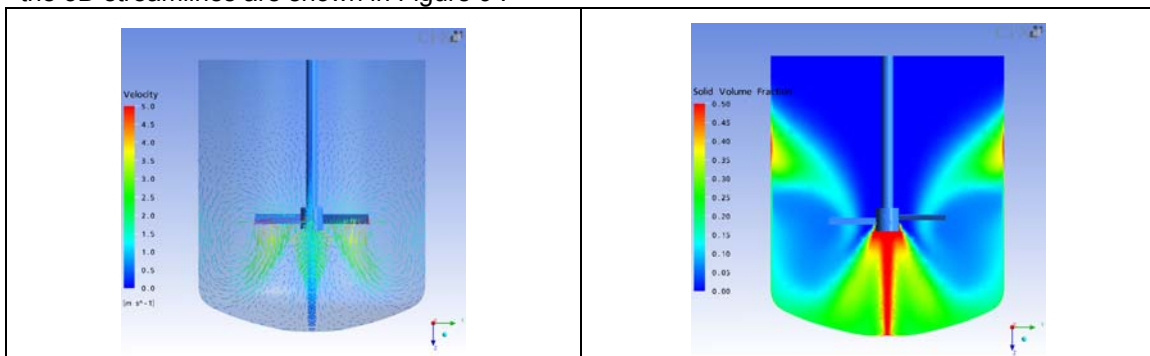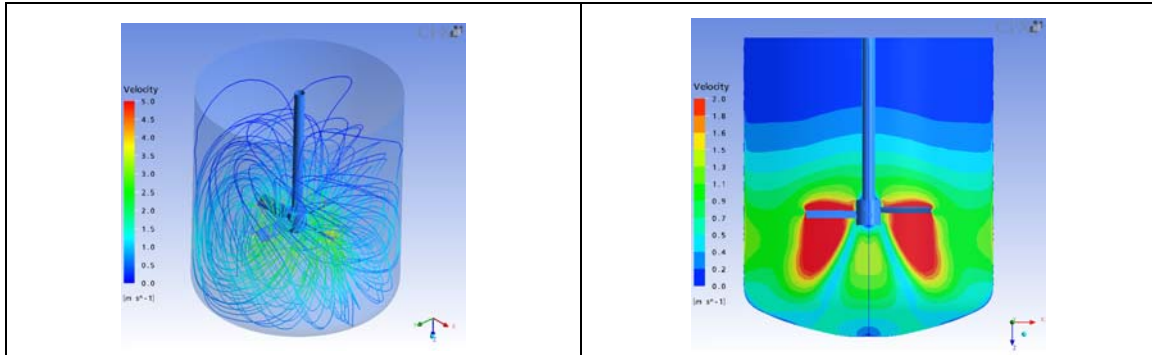
Figure 9 – Initial Design – 45º Pitched Blade Impeller

The optimized impeller has a high discharge angle, resulting in a higher pumping effectiveness and a higher solid suspension. Figure 10 shows the velocity vector plot, the solid concentration distribution, the velocity distribution and the 3D streamlines for the proposed impeller. The solid concentration in the bottom of the vessel is very low, resulting in a low variance and results also show very well homogenized suspension.
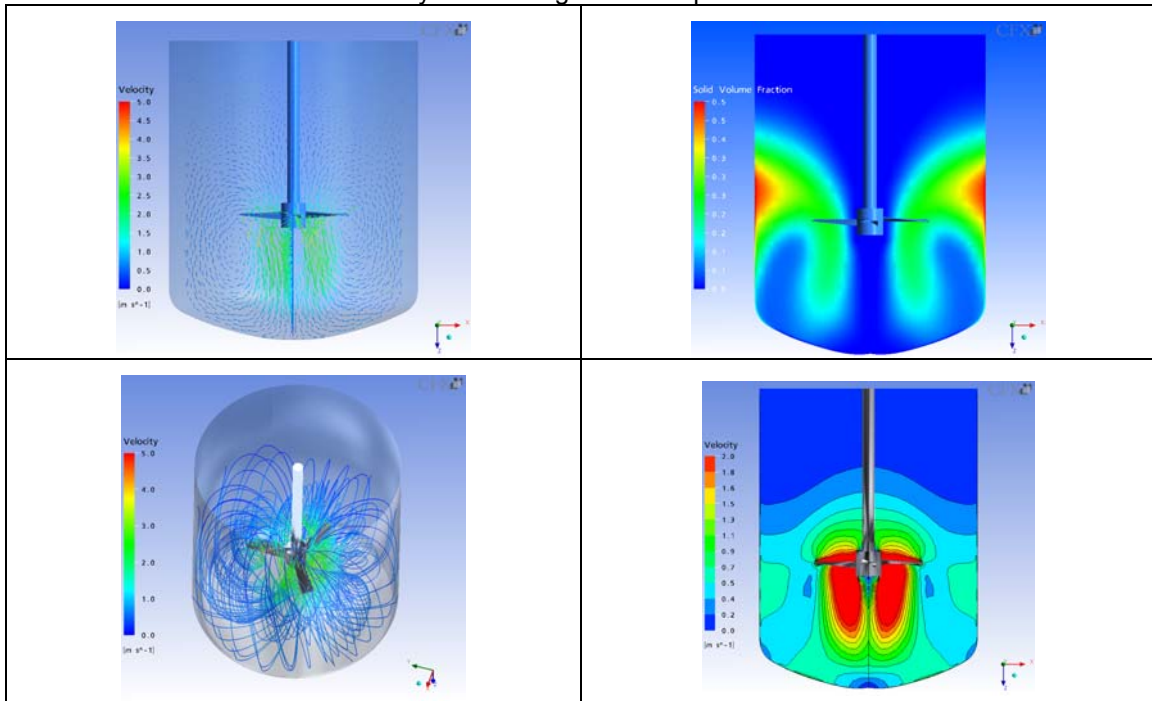

Figure 10 – Optimized Impeller

Before the optimization steps using modeFRONTIER, an impeller tip was designed in order to reduce the induced drag and the tip vortex. A smooth joining between the impeller blade and the hub was designed to reduce the boundary layer separation on this region and improve the blade suction. The final impeller design is shown in Figure 11.
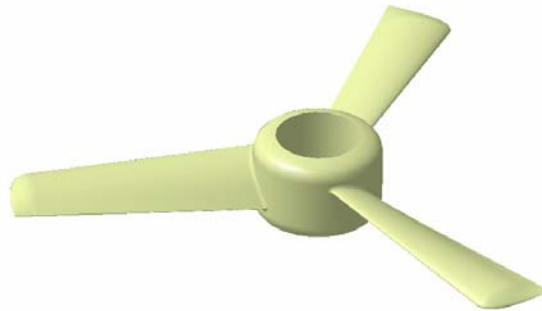
Figure 11 – Optimized Blade Design

5. Summary and conclusions

The multi-objective optimization procedure for an optimal impeller design contains many innovative elements, especially if consideration of the small number of generated prototypes is considered.

It is believed that the incorporation of parameterization refinements such as tip construction and smoothness on the impeller surface helped in achieving better results. Nevertheless, the main objective of this research was both to show that an optimization process is viable for determining optimal designs and a brief outline of the method has been presented.

This work also indicated the advantages of coupling Computational Fluid Dynamics and Multi-Objective Design Optimization methods.

6. Acknowledgements

7. References

[1]   B.T. Neyer (1992), "Analysis of Sensitivity Tests," MLM-3736, EG&G Mound Applied Technologies, Miamisburg, Ohio

[2]   B. T. Neyer (1994), "A D-Optimality-Based Sensitivity Test," Technometrics, 36, pp. 61-70.

[3]   Bakker A., et al., "Realize Greater Benefits from CFD," Chem. Eng. Progress, 97 (3), pp. 45–53 (Mar. 2001).

[4]   Bakker, A., and J. B. Fasano, "Time Dependent, Turbulent Mixing and Chemical Reaction in Stirred Tanks," paper presented at AIChE Annual Meeting, St. Louis, MO (Nov. 1993), also published in "AIChE Symposium Series," No. 299, 90, "Industrial Mixing Technology: Chemical and Biological Applications," G. B. Tatterson, volume editor, pp. 71–78 (1994).

[5]   Buurman, C., G. Resoort and A. Plaschkes, "Scaling-up Rules for Solids Suspension in Stirred Vessels", Chem. Eng. Sci. 41, 2865–2871 (1986).

[6]   Drewer, G.R., N. Ahmed and G.J. Jameson, "Suspension of High Concentration Solids in Mechanically Stirred Vessels", IChemE Symp. Series No. 136 (Proc. 8th European Conf. on Mixing), (1994), pp. 41–48.

[7]   Fox, R. O., "On the Relationship between Lagrangian Micromixing Models and Computational Fluid Dynamics," Chem. Eng. And Proc., 37, pp. 521–535 (1998).

[8]   Green, D.W. and J.O. Maloney, Perry's Chemical Engineers' Handbook," 7th ed., Eds., McGraw-Hill, New York (1997).

[9]   Hicks, M.T., K.J. Myers and A. Bakker, "Cloud Height in Solids Suspension Agitation", Chem. Eng. Comm. 160, 137–155 (1997).

[10]   Ibrahim, S. and A.W. Nienow, "Particle Suspension in Turbulent Regime: The Effect of Impeller Type and Impeller/Vessel Configuration", Trans IChemE 74(A), 679–688 (1996).

[11]   J.B. Fasano, A. Bakker, and W.R. Penney, Advanced impeller geometry boosts liquid agitation, Advanced Liquid Agitation, Chemineer, May (1999) reprinted with permission from Chemical Engineering'

[12]   J.H. Rushton, E.W. Costich, and H.J. Everett, Power Characteristics of Mixing Impellers, Part II, Chem. Eng. Prog., Vol 46, No.9, (1950), pp. 467-476

[13]   J. W. Dixon and A. M. Mood (1948), "A Method for Obtaining and Analyzing Sensitivity Data," Journal of the American Statistical Association, 43, pp. 109-126.

[14]   Menter, F.R.: Two-Equation Eddy-Viscosity Turbulence Models for Engineering Applications, AIAA Journal, Vol. 38, pp. 1598 – 1605, 1994.

[15]   modeFRONTIER: The   Multi-Objective   Optimization   and   Design   Environment, http://www.esteco.it

[16]   Mordecai Avriel (2003). "Nonlinear Programming: Analysis and Methods." Dover Publishing. ISBN 0-486-43227-0.

[17]   Myers, K.J. and A. Bakker, "Solids Suspension with Up-pumping Pitched-blade and High-efficiency Impellers", Can. J. Chem. Eng. 76, 4233-440 (1998).

[18]   Nienow, A.W., "The Suspension of Solid Particles", in "Mixing in the Process Industries", 2nd ed, N. Harnby, M.F. Edwards and A.W. Nienow, Eds., Butterworths, London, UK (1992), pp. 364–393.

[19]   Nienow, A.W., M. Konno and W. Bujalski, "Studies on Three-phase Mixing: A Review and Recent Results", in "Proc. 5th European Conf. on Mixing", Wurzburg, West Germany, June (1985), pp. 1–13.

[20]   Panos Y. Papalambros and Douglass J. Wilde (2000). Principles of Optimal Design: Modeling and Computation, Cambridge University Press. ISBN 0-521-62727-3.

[21]   Pantula, P.R.K. and N. Ahmed, "The Impeller Speed Required for Complete Solids Suspension in Aerated Vessels: A Simple Correlation?", in "Récents progres en genie des procédés (Mixing IX)", Paris, France (1997), pp. 11–18.

[22]   Pantula, P.R.K. and N. Ahmed, "Solids Suspension and Gas Holdup in Three Phase Mechanically Agitated Reactors", in "Chemeca '98", Port Douglas, Queensland, Australia, (1998), Paper No. 132.

[23]   Paul, E.L., et al., "Handbook of Industrial Mixing, Science & Practice", Eds., Wiley, Hoboken, N.J. (2004).

[24]   R.J. Weetman and J.Y. Oldshue, Comparison of Mass Transfer Characteristics of Radial and Axial Flow Impellers, 6th European Conference on Mixing, Pavia, Italy, ISBN 0 947711 33 3, May 24-26, (1988)

[25]   R.J. Weetman, Process/Mechanical Design Aspects for Lightnin A315 Agitators in Minerals Oxidation, Randol Gold 1993, Beaver Creek, USA, (1993), pp. 247-253

[26]   R.J. Weetman and C.K. Coyle, The Use of Fluidfoil Impellers in Viscous Mixing Applications, AIChE 1989 Annual Meeting, San Francisco, USA, Nov. 5-10, (1989)

[27]   Raghava Rao, K.S.M.S., V.B. Rewatkar and J.B. Joshi, "Critical Impeller Speed for Solid Suspension in Mechanically Agitated Contactors", AIChE J. 34, 1332–1340 (1988).

[28]   Rewatkar, V.B., K.S.M.S. Raghava Rao and J.B. Joshi, "Critical Speed for Solid Suspension in Mechanically Agitated Three-Phase Reactors: 1. Experimental Part", Ind. Eng. Chem. Res. 30, 1770–1784 (1991).

[29]   Stephen Boyd and Lieven Vandenberghe (2004). Convex Optimization, Cambridge University Press. ISBN 0-521-83378-7.

[30]   Wilcox, D.C.: Turbulence Modeling for CFD, DCW Industries, 2nd ed., 1998.

[31]   Wilcox, D.C.: Reassessment of the Scale-Determining Equation for Advanced Turbulence Models, AIAA Journal, Vol. 26, pp. 1299 – 1310, 1988.

[32]   Wong, C.W., J.P. Wang and S.T. Huang, "Investigations of Fluid Dynamics in Mechanically Stirred Aerated Slurry Reactors", Can. J. Chem. Eng. 65, 412–419 (1987).

[33]   Wu, J., Y. Zhu, P.C. Bandopadhayay, L. Pullum and I.C. Shepherd, "Solids Suspension with Axial Flow Impellers", AIChE J. 46, 647–650 (2000).

[34]   Wu, J., Y. Zhu and L. Pullum, "The Effect of Impeller Pumping and Fluid Rheology on Solids Suspension in a Stirred Vessel", Can. J. Chem. Eng. 79, 177–186 (2001).

[35]   Zwietering, Th.N., "Suspending of Solid Particles in Liquid by Agitators", Chem. Eng. Sci. 8, 244–253 (1958).

[36]   Zhou, W., et al., "Application of CFD in Modeling Multiphase Reactors," paper presented at Chemical Reaction Engineering VII: Computational Fluid Dynamics, Quebec City, Canada — sponsored by the United Engineering Foundation, New York — (Aug. 6–11, 2000).

8.   Appendix 1 - Documentation

Throughout this article, dimensions are given in terms of the fundamental magnitudes of length (L), mass (M), time (T). This section lists symbols used in this paper, their meaning, dimensions and, where applicable, their values. Dimensionless quantities are denoted by 1. The values of physical constants (or their default values) are also given.

Symbol	Description	Dimensions	Value
$C_{\varepsilon 1}$	k-ε Turbulence model constant	1	1.44
$C_{\varepsilon 2}$	k-ε Turbulence model constant	1	1.92
C_{μ}	k-ε Turbulence model constant	1	0.09
E	Constant used for near-wall modelling	1	9.793
g	Gravity vector	$L\,T^{-2}$	9.81
k	Turbulence kinetic energy per unit mass	$L^2\,T^{-2}$	
P_k	Shear production of turbulence	$M\,L^{-1}\,T^{-3}$	
p, p_{stat}	Static (thermodynamic) Pressure	$M\,L^{-1}\,T^{-2}$	
p_{ref}	Reference pressure	$M\,L^{-1}\,T^{-2}$	
p_{tot}	Total pressure	$M\,L^{-1}\,T^{-2}$	
p'	Modified Pressure	$M\,L^{-1}\,T^{-2}$	
R_e	Reynolds Number	1	
r	Location vector	L	
S$_M$	Momentum source	$M\,L^{-2}\,T^{-2}$	
S_{ct}	Turbulent Schmidt Number, $\mu_t\,/\,\Gamma_t$	1	
U	Vector of velocity $U_{x,y,z}$	$L\,T^{-1}$	

U	Velocity magnitude	$L\,T^{-1}$	
u	Fluctuating velocity component in	$L\,T^{-1}$	
ε	Turbulence dissipation rate	$L^2\,T^{-3}$	
ζ	Bulk viscosity	$M\,L^{-1}\,T^{-1}$	
κ	Von Karman constant	1	0.41
μ	Molecular (dynamic) viscosity	$M\,L^{-1}\,T^{-1}$	
μt	Turbulent viscosity	$M\,L^{-1}\,T^{-1}$	
μeff	Effective viscosity, $\mu+\mu t$	$M\,L^{-1}\,T^{-1}$	
ρ	Density	$M\,L^{-3}$	
σk	Turbulence model constant for the k	1	1.0
$\sigma \varepsilon$	k-ε Turbulence model constant	1	1.3
σw	k-ω Turbulence model constant	1	2
τ	Shear stress or sub-grid scale stress	$M\,L^{-1}\,T^{-2}$	
ω	Angular velocity	T^{-1}	
y^+	Yplus	1	

P	Power Consumption		
N	Rotational speed	T^{-1}	
N_p	Power Number	1	
N_q	Pumping Number	1	
D	Impeller Diameter	L	
T	Tank diameter	L	
C	Bottom clearance	L	
H	Height of the liquid	L	